Rapid Interchangeable Hydrogen, Hydride and Proton Species at the Interface of Transition Metal Atom on Oxide Surface

Simson Wu,[1] Kai-Yu Tseng,[2] Ryuichi Kato,[3] Tai-Sing Wu,[4,5] Alexander Large,[6] Yung-Kang Peng,[7] Weikai Xiang,[8] Huihuang Fang,[1] Jiaying Mo,[1] Ian Wilkinson,[9] Yun-Liang Soo,[4,5] Georg Held,[6] Kazu Suenaga,[3] Tong Li,[8] Hsin-Yi Tiffany Chen[2,] and Shik Chi Edman Tsang[1*]*

[1]The Wolfson Catalysis Centre, Department of Chemistry, University of Oxford, Oxford, OX1 3QR, UK
[2]Department of Engineering and System Science, National Tsing Hua University, Hsinchu 300044, Taiwan
[3]National Institute of Advanced Industrial Science and Technology (AIST), Central 5, 1-1-1 Higashi, Tsukuba 305-8565, Japan
[4]National Synchrotron Radiation Research Center, Hsinchu 300, Taiwan
[5]Department of Physics, National Tsing Hua University, Hsinchu 300044, Taiwan
[6]University of Reading, Whiteknights, Reading, Berkshire, RG6 6AH, UK
[7]City University of Hong Kong, Hong Kong
[8]Institute for Materials, Ruhr-Universität Bochum, 44803, Bochum, Germany
[9]Siemens plc, CT NTF, Wharf Road, Oxford OX29 4BP, UK

Supporting information

Supplementary methods

1. Experimental procedures

Chemicals and Materials

$Mg(NO_3)_2$, $MgCl_2 \bullet 6H_2O$ (reagent grade), benzoic acid, sodium hydroxide (reagent grade), $Ru_3(CO)_{12}$, THF (anhydrous, >99.9%) were from Sigma-Aldrich. High purity hydrogen gas (99.99%), nitrogen gas (99.99%), argon gas (99.99%), dilute oxygen gas (2.5% O_2 in He), dilute hydrogen gas (5% H_2 in N_2) were obtained from BOC. Purity of hydrogen and nitrogen was further enhanced with oxygen, carbon dioxide and moisture traps (HP and 5 Å) attaching to the gas cylinders.

Materials Synthesis

MgO preparation

MgO(110) was prepared by the calcination under vacuum method. Typically, commercial MgO (500 mg) was boiled in deionised water for 5 hours. The raw product was then collected by centrifugation and was subsequently dried at 120 ^oC for 12 hours. The product was calcined under vacuum at 500 ^oC for 6 hours [1,2]. MgO(111) was synthesized using the hydrothermal method with the aid of benzoic acid as surfactant. Typically, $MgCl_2 \bullet 6H_2O$ (2 g) and benzoic acid (0.12 g) was dissolved in 60mL deionised water. The mixture was stirred for 1 hour. 2M NaOH (20 mL) was then added drop wise into the solution, forming a white precipitate. The slurry was subsequently transferred to a 100mL autoclave and gradually heated to 180 ^oC and maintained at this temperature for 24 hours. The $Mg(OH)_2$ precursor was obtained after filtration followed by washing with water and drying at 80 ^oC under vacuum overnight. Refined synthesis of MgO(111) nanosheets of optimal surface areas were obtained after calcination in compressed air at 500 ^oC for 6 hours [1,3–8].

Preparation of Ru/Mg(111) and Ru/MgO(110)

Typically, $Ru_3(CO)_{12}$ was dispersed in THF for 2 hours under sonication. The mixture was then transferred to the MgO or activated carbon (AC) and allowed to stir at ambient temperature for 8 hours where the solvent is subsequently removed by rotary evaporation. The obtained powder was dried in a 70 ^oC oven for 12 hours under vacuum. After that the powder is transferred to a temperature-programmed furnace and heated to 350 ^oC for 6 hours under Ar stream to remove the CO ligand from the Ru precursor. Loading of Ru on MgO(111) and MgO(110) was confirmed to be 3.4 weight % and 3.7 weight% using ICP-MS.

Characterisation techniques

Computational details.

The spin-polarised DFT calculations were performed using the *Vienna ab initio Simulation Package* (*VASP*) [9–11] software. The generalized gradient approximation (GGA) based Perdew-Burke-Erzerhof (PBE) functional [12] was used to include the exchange and correlation effect of the valence electrons. The kinetic energy cutoff of 450 eV was used for all calculations. The project-augmented wave (PAW) [13,14] method was used to describe the core–valence electron interactions. Each atoms was relaxed until the Hellman−Feynman force criterion were less than 0.01 eV/Å by using the conjugate gradient minimization algorithm. The bulk structure was optimized using a 10 × 10 × 10 Gamma centered grid of *k*-points mesh. The calculated lattice parameters of the bulk MgO is 4.249 Å, which are very close to the corresponding experimental values of 4.21 Å (calculated from XRD using Bragg's Law).

The pure MgO(111) surface was modeled using a twelve-layer slab repeated in a 2 × 2 surface unit cell; Symmetric slab model was considered for optimization by fixing the middle four layers to balance the dipole-moment. The *k*-point mesh was sampled using a 1 × 1 × 1 Gamma centered grid. To avoid interactions between slabs, all slabs were separated by a vacuum gap greater than 15 Å. After complete convergence testing studies, the geometric and electronic structures of the slabs are analyzed. The charge transfer was investigated with Bader charge analysis. We used a Gaussian smearing with σ = 0.01 eV for Density of state analysis.

The H adsorption energy (E_{ads}) on the clean substrate was calculated by:

$$E_{ads} = E(_{H/sub}) - E(_{sub}) - ½E(_{H2}),$$

where $E(_{H/sub})$, $E(_{sub})$, and $E(_{H2})$ are the DFT energies of the adsorption complex, clean substrate, and gas-phase H_2 molecule, respectively.

The H adsorption energy on Ru/MgO was calculated by:

$$E_{ads} = \{E_{(nHRu/MgO)} - E_{(Ru/MgO)} - n/2E_{(H2)}\}/n$$

where $E_{(nHRu/MgO)}$, $E_{(Ru/MgO)}$, and $E(_{H2})$ are the DFT energies of the adsorption complex, main catalyst, and gas-phase H_2 molecule, respectively while n is number of H atoms.

The binding energy of Ru atom on MgO surfaces was calculated by:

$$E_b = E_{(Ru/MgO)} - E_{(Ru)} - E_{(MgO)} \text{ (w.r.t. Ru atom)}$$

where $E_{(Ru/MgO)}$, $E_{(MgO)}$, and $E_{(Ru)}$ are the DFT energies of the adsorption complex, clean substrate, and Ru atom in gas-phase, respectively.

In-situ XPS measurements

The study of the Ru charge distribution and the corresponding change in [OH] concentration under different gas conditions was performed by means of operando XPS measurements, at the Diamond Light Source B07 beamline. The powdered samples were dissolved in acetone and mounted on a silicon wafer, which were subsequently heated by a heat plate at 110 ^{o}C to remove the solvent. The temperature was maintained at a constant throughout the experiment at 350 °C. The measurements were performed either under 1 mbar Ar or 1 mbar H_2. The gas composition was continuously monitored by online mass spectrometry (MS). If not otherwise stated, Ru 3d, O 1s, and Mg 2s spectra were recorded using a fixed photon energy of 950 eV. The binding energy (BE) scale was calibrated with respect to the Mg 2s (88.1 eV) as internal standard.

In-situ FTIR measurements

The Fourier-Transform Infra-Red (FTIR) experiments were carried out using a Thermo Scientific Nicolet 6700 spectrometer equipped with CaF2 windows at 200 ^{o}C. Spectra were obtained by collecting 32 scans with a resolution of 4 cm^{-1} and are presented in absorbance unit. Powder of freshly prepared samples were pressed into pellets and loaded onto the sample holder. The sample was then flushed with He for 30 minutes to clean the surface under 250 ^{o}C followed by ramping down to 200 ^{o}C for measurement. After collecting background spectra, N_2 gas was passed through the sample holder for 15 minutes at 20 mL min^{-1} and in-situ sample spectra were recorded. After 15 minutes, H_2 gas was then passed at 20 mL min^{-1} and in-situ spectra were recorded. The presented spectra are the difference spectra between the in-situ spectra and the background spectra.

APT measurements

APT relies on generating high electric fields (~3–5 V $Å^{-1}$) at the apex of a needle-shaped specimen. On top of this, an additional short (ns) voltage or laser pulse was applied to remove ions in a controlled manner into a high-resolution time-of-flight mass spectrometer equipped with a single-ion-sensitive detector. APT thus can provide 3D elemental mapping with single-atom sensitivity.

To prepare the APT specimens, nanoparticles were first distributed on a Ni-coated Si flat wafer and subsequently embedded by a 150-nm thick protective Ni layer in Leica EM ACE600 high vacuum sputter coater[4]. The needle-shaped APT specimens were then prepared by a standard lift-out procedure using a focused ion beam/scanning electron microscope (FIB/SEM) in FEI G4 CX. The APT experiments were conducted in a CAMECA LEAP 5000 XR instrument at a specimen temperature of 50 K, a detection rate of 0.5, a pulsing rate of 125 kHz, and a laser pulse energy of 30 pJ. Data reconstruction and analysis were performed using the commercial IVAS 3.8.2™ software.

^{1}H NMR measurements

Static ^{1}H MAS NMR spectra were taken to investigate the hydrogenic species on MgO(111) and Ru-MgO(111), respectively after their pre-reduction in H_2. Before data collection, samples

were pretreated using the following procedure. They were first placed in glass tubes connected to a vacuum line or H_2 gas at 350 ^oC for 1 h. After pre-reduction in flowing H_2 in 1 atmosphere, the samples were cooled to room temperature, Ar gas was introduced to the samples. Sample tubes were sequentially flame-sealed and transferred into a ZrO_2 rotor with a kel-F end-cap in a glovebox. NMR measurements were carried out at 298 K using a Bruker Avance III 400 MHz spectrometer at the Larmor frequencies of 399.33 for ^1H.

Synchrotron X-ray absorption fine structure (XAFS)

XAFS spectra for the Ru/MgO(111) sample was recorded at the Ru K absorption edge, in fluorescence mode using a Lytle fluorescence detector, under reaction conditions, at beamline BL07A of the Taiwan light source at National Synchrotron Radiation Research Center in Taiwan. A Si (111) Double Crystal Monochromator(DCM) was used to scan the photon energy. The energy resolution for the incident X-ray photons was estimated to be 2×10^{-4}. The Demeter software package (Athena and Artemis) was used for XAFS data analysis for the Ru data. To ascertain the reproducibility of the experimental data, at least two scan sets were collected and compared for each ex-situ sample. The spectra were calibrated with foils as a reference. And the amplitude parameter was obtained from EXAFS data analysis of the Ru foil, which was used as a fixed input parameter in the data fitting to allow the refinement in the coordination number of the absorption element. In this work, the first shell data analyses under the assumption of single scattering were performed with the errors estimated by R-factor.

For the in-situ measurements the spectrum was obtained in fluorescence mode using a fixed bed reactor with Kapton windows to allow synchrotron X-rays to pass through. The temperature was controlled with a Eurotherm controller with a thermocouple positioned in the centre of the heating block. For safety reasons, dilute gas mixtures were used. H_2/He (5% H_2 balanced in He, BOC) and pure He gases were introduced to the heated chamber containing the fixed bed of catalysts with flow rates controlled by mass flow controllers. The reactor was heated to 300 °C at a ramp rate of 5 °C/min and held at temperature for 30 min under a flow of H_2/He for pre-reduction. Then it was switched to He and flowed for 30 minutes. XAFS spectrum was then obtained until there is no change in the absorption edge.

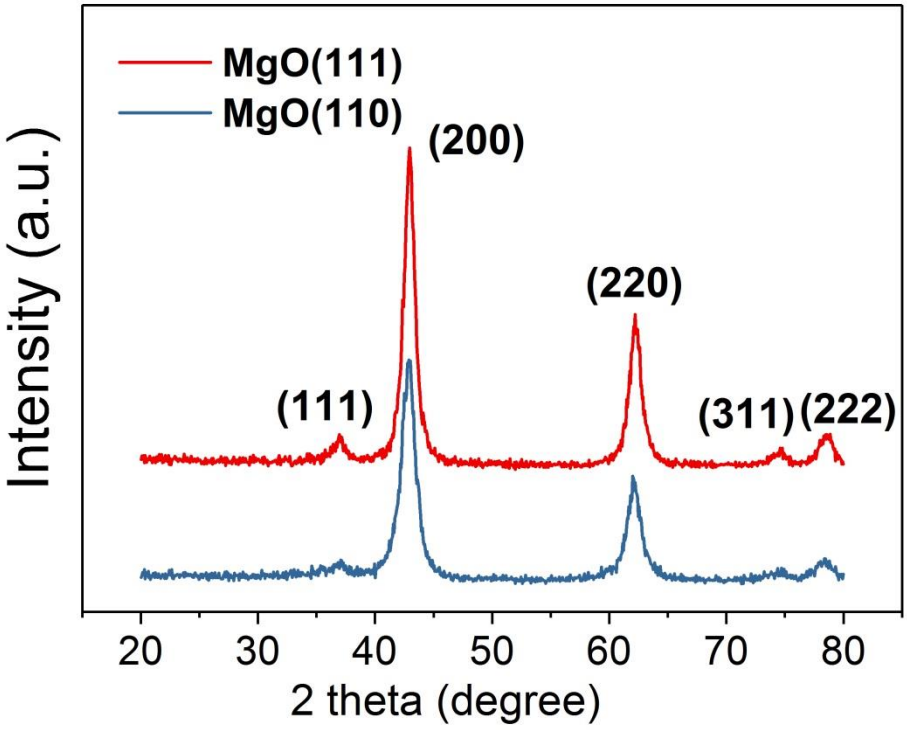

Figure S1. Phase identification of MgO(111) and MgO(110) confirmed by X-ray diffraction.

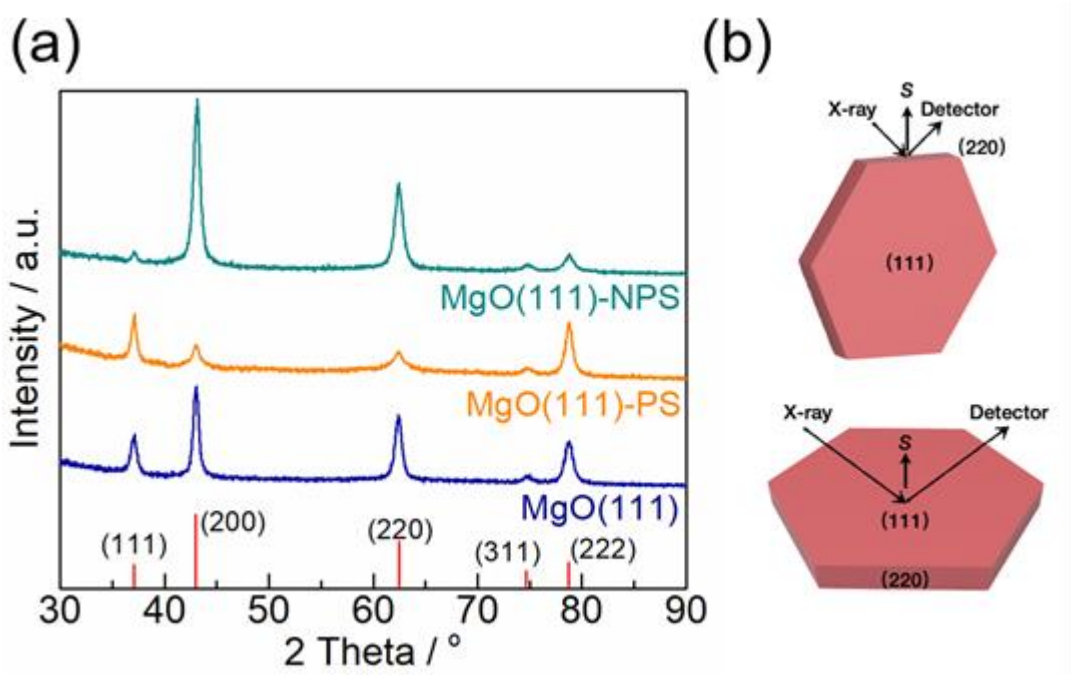

Figure S2 (a) XRD patterns of MgO(111) with no dispersion [MgO(111)], ethanol-dispersion [MgO(111)-PS], and n-hexane-dispersion [MgO(111)-NPS]. PS stands for polar solvent (ethanol) whereas NPS stands for non-polar solvent (hexane); **(b)** schematic illustration of MgO nanosheets where X-ray beams incident at different exposed facet. Top panel: diffraction vector is parallel to the (111) facet; Bottom panel: diffraction vector is perpendicular to the (111) facet.

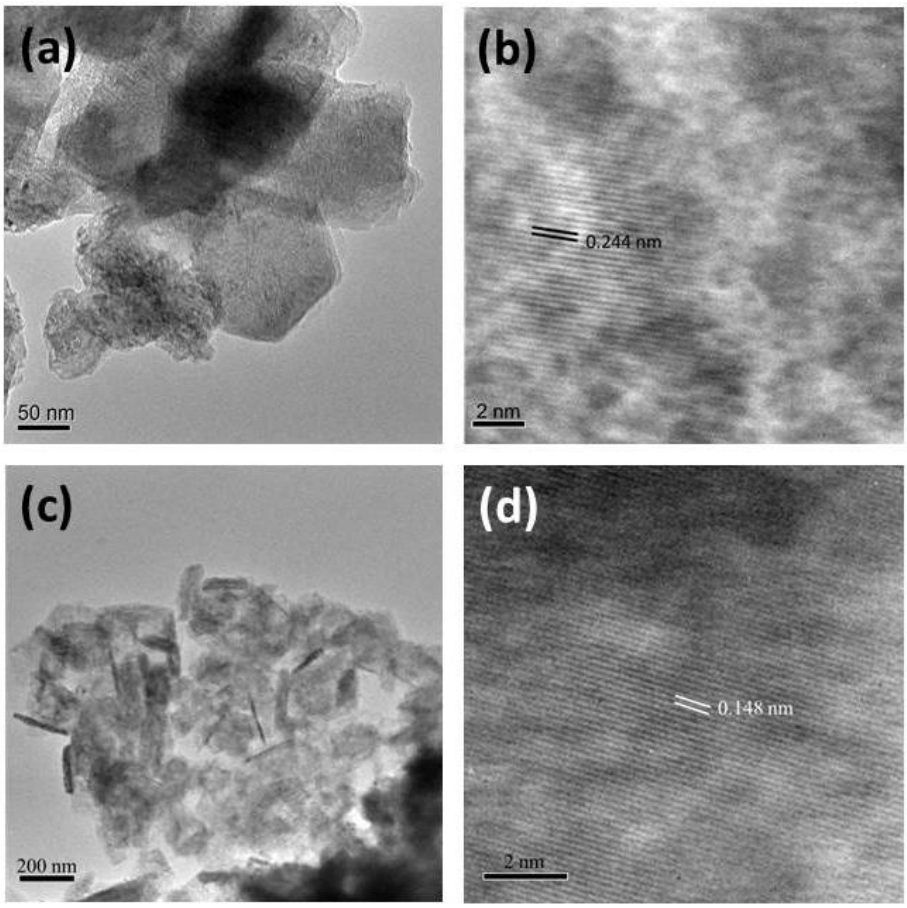

Figure S3. TEM and HRTEM images of (a-b) MgO(111), (c-d) MgO(110). Lattice spacing on each exposed plane is calculated from the average of 10 lattice spacing. Both of the values for MgO(111) and MgO(110) matches well with the literature[7,8].

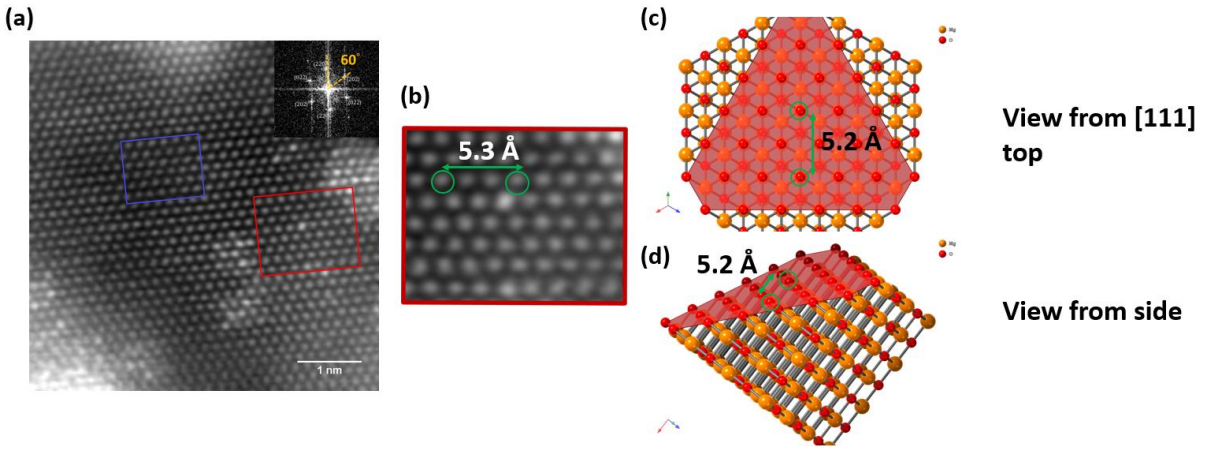

Figure S4. (a) HAADF-STEM image of 3.4 wt%-Ru/MgO(111) observed from [111] direction. The bright spots are confirmed to be Ru from EELS; individual Ru on trigonal OOO hollow sites and 2-D islands with no Ru-Ru lattice formed probably via surface Ostwald ripening can be seen. The inset in (a) displays the corresponding FFT pattern of the pure faceted MgO(111) region in the blue rectangle; **(b)** Enlarged pattern of the region in the red rectangle in (a). The distance between 4 oxygen atoms is measured to be 5.3 ± 0.2 Å; **(c)** Simulated model of MgO(111) with exposed oxygen-terminated surface (Red: O, Orange: Mg). The view direction is from [111]. The [111] lattice plane (red) is displayed for reference. The distance between 4 atoms (2 atoms in the [111] plane and 2 atoms are from layers below) is 5.2 Å: thus, the pattern and the distance match well with the measured value in the experimental STEM image; **(d)** The side view of the MgO(111) model in (c).

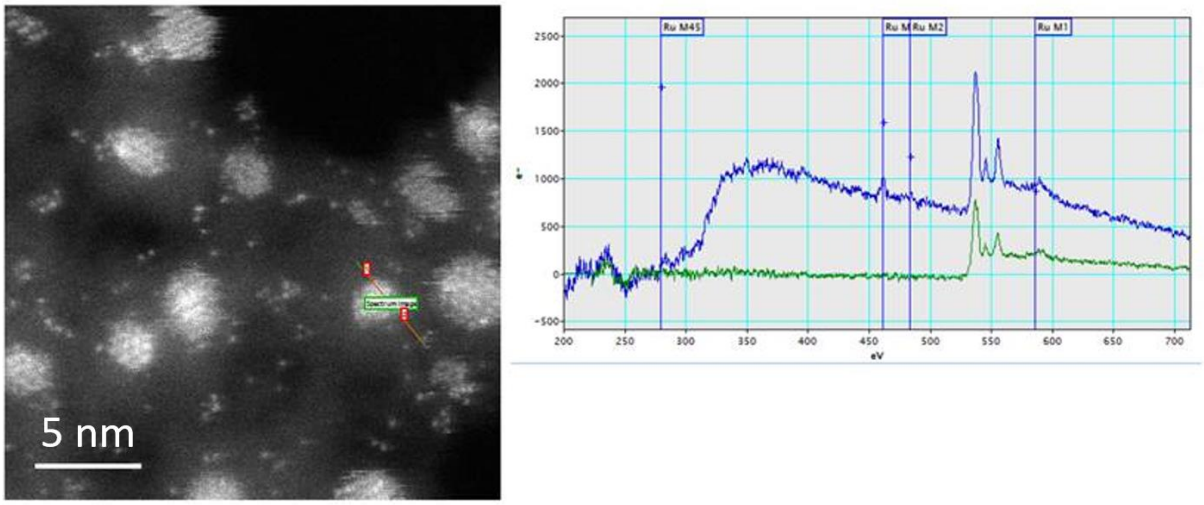

Figure S5. STEM image of Ru/MgO(110). The presence of Ru is identified by EELS mapping. All the Ru species are in the form of nanoparticles (nps) with matched Ru-Ru metal lattice. The tiny white dots shown in the image might possibly be due to contamination since EELS displays no signal for the Ru M edges in contrast to the nanoparticles. The exposed plane where Ru nps were sitting on was however not clearly defined, which might be caused by significant charging effect due to the insulator nature.

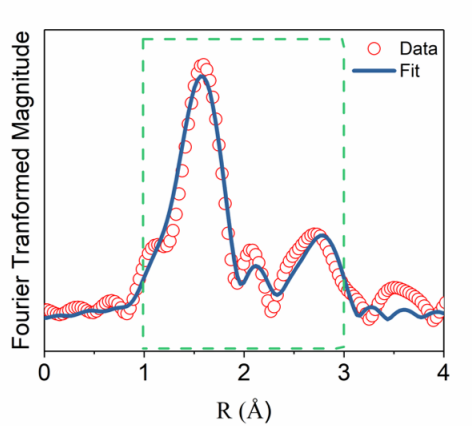

Scattering Path	Bond Length (Å)	Coordination No.	Debye Waller's factor
Ru-O	2.03 (2)	3.0 (2)	0.009
Ru-Mg	3.17 (3)	1.4 (3)	0.003

Figure S6. Fourier Transformed of Ru K-edge EXAFS spectra for Ru/MgO(111) measured at 300 ºC under flowing He after hydrogen pre-reduction. Parameters obtained from least-square fitting are shown on the right. Parameters used: k-range: 3-12, R-range: 1-3, R-factor: 1.9%.

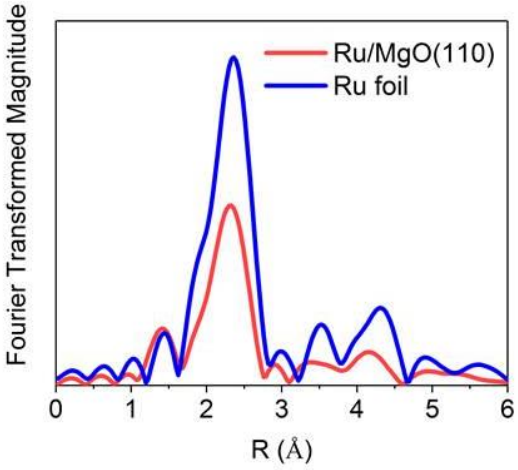

Least square fitting for Ru-MgO(110):

Scattering path	Bond Length (Å)	Coordination No.	Debye-Waller factor
Ru-Ru	2.68 (3)	6.1 (4)	0.004 (1)

Figure S7. Fourier Transformed of Ru K-edge EXAFS spectra for Ru/MgO(110) and Ru(0) foil at ambient temperature. Parameters obtained from least-square fitting are shown on the right. Parameters used: k-range: 3-11.4, R-range: 1.35-3, R-factor: 2.0%.

Initial Structure	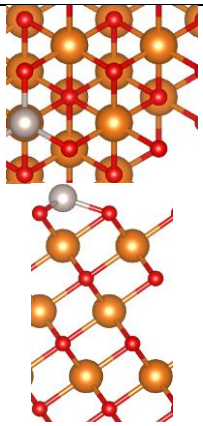 O Hollow site atop Mg	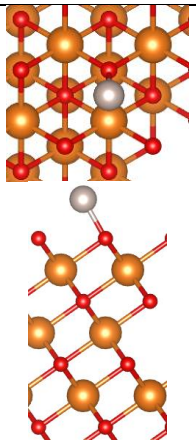 O-Mg Bridge site	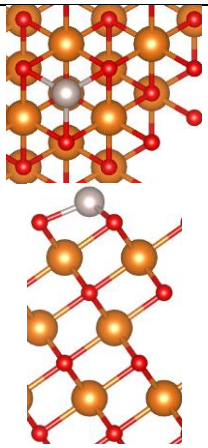 O Hollow site atop O	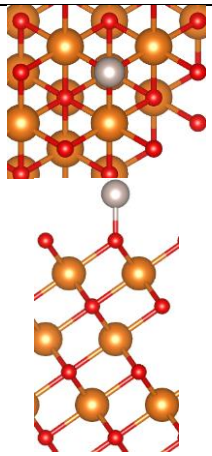 Atop O site
Optimized Structure	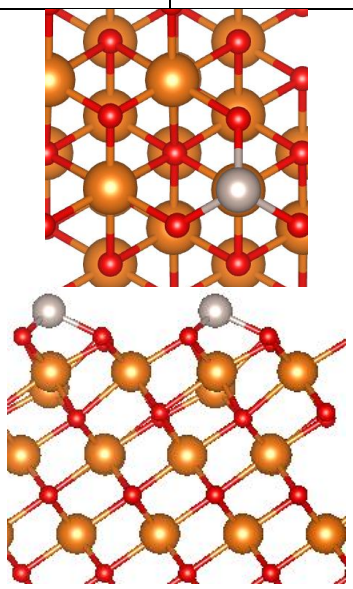 **O Hollow site atop to Mg**		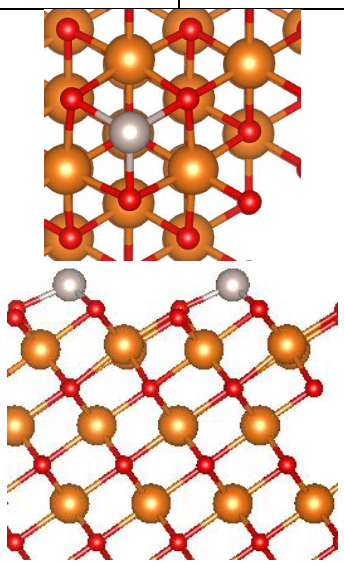 O Hollow site atop O	
E_{ads} (eV)	-10.81		-10.75	
Average d(Ru-O) (Å)	1.812		1.840	

Figure S8. Density Functional Theory calculations give the optimised geometry of a single Ru atom on hollow OOO atop to Mg as the most stable surface site of MgO(111).

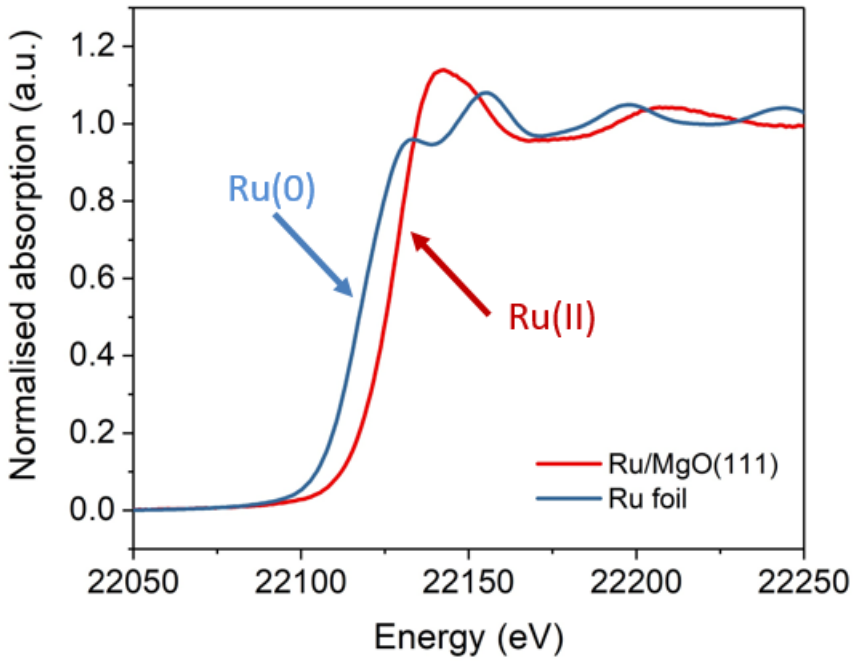

Figure S9. In-situ XANES measured at 300 ^{o}C under flowing He. The shift towards higher binding energy indicates a positive oxidation state of Ru.

(a)

System			MgO (111)	Ru / MgO (111)	MgO (110)	Ru / MgO (110)
Adsorption Site			-	O-O-O Hollow atop Mg	-	O-O Bridge atop Mg
E_{bind} (eV)			-	-10.81	-	-3.18
q|e|	**Ru**		-	+ 1.270	-	- 0.238
	Over layer	**O bind with Ru**	-	-1.050	-	-1.447
		O no bind with Ru	-0.971	-1.504	-1.576	-
		Mg	+1.633	+1.637	+1.603	+1.574
	O unfixed in bulk		-1.643	-1.640	-1.634	-1.636
	O fixed in bulk		-1.655	-1.655	-1.631	-1.631
	Mg unfixed in bulk		+1.640	+1.641	+1.628	+1.632
	Mg fixed in bulk		+1.655/ -	+1.655	+1.631	+1.631
	Bottom layer	**Mg**	+1.076	+1.064	+1.603	+1.575
		O	-1.830	-1.860/ -	-1.583/ -	-1.583
	Total MgO		0.000	-1.270	0.000	+0.238

(b)

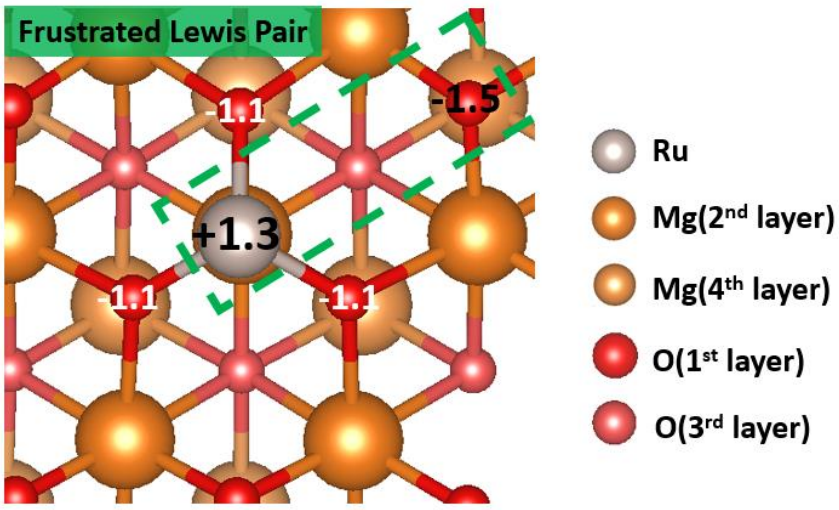

Figure S10. (**a**) Bader charge analysis of surface Ru and O on the Ru/MgO(111); (**b**) Optimised structure of Ru/MgO(111) depicting the charge on the surface atoms.

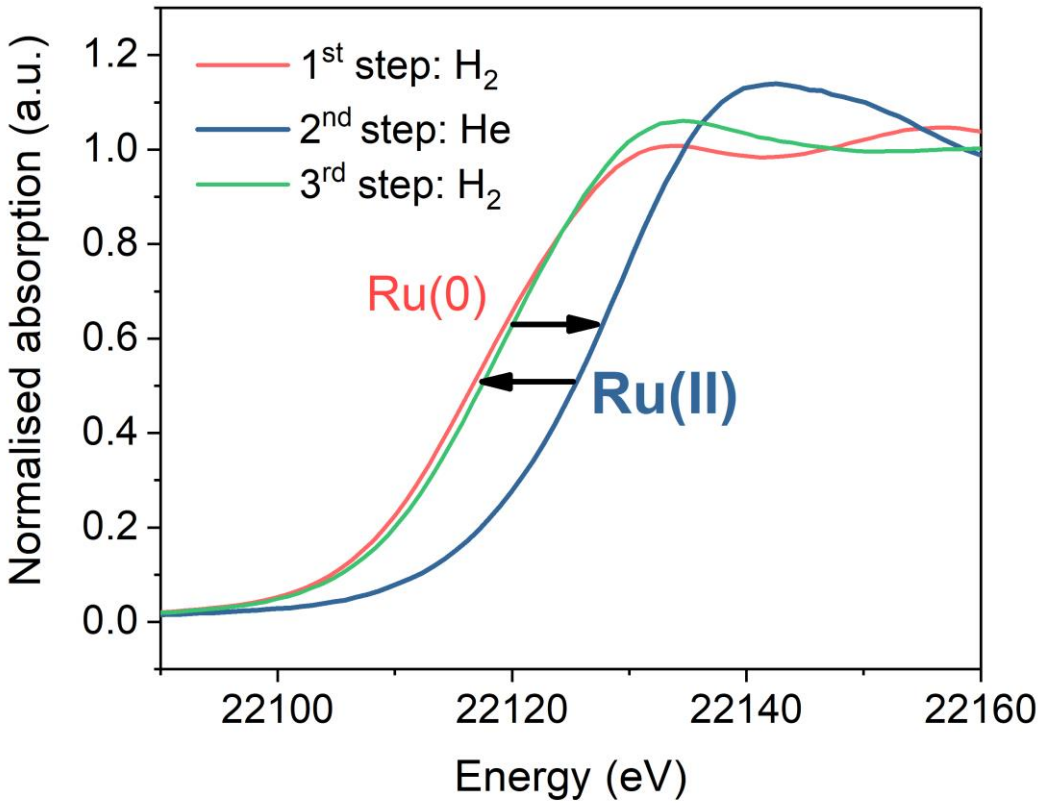

Figure S11. In-situ XANES for Ru/MgO(111) under dynamic switching between 5%H_2/He and He at 300 ^oC.

The XANES spectra for Ru K-edge (of the Ru-MgO(111) sample) indicates a zero oxidation state when it is under hydrogen, but quickly swings towards higher binding energy upon switching from hydrogen to helium. This suggests an increase in the oxidation state for the Ru when the sample is out of the reducing atmosphere. As a result, a continuous driving force is needed to keep the Ru at a reduced state with corresponding coverage of H^+ on the oxide support surface. In our case, under a hydrogen atmosphere, the forward hydrogen spillover process causes the adsorbed hydrogen atom to split into proton that migrate towards the oxygen-terminated surface of the support and electron that reduces the Ru^{2+} to Ru(0). When the hydrogen atmosphere is removed, the hydroxyl proton on the support undergoes reverse-spillover where the H^+ abstracts the electron from Ru and becomes H atom again. This echoes with the AP-XPS experiment showing a reduction in the [OH] shoulder and corresponding increase in the [O^{2-}] component when the gas feed is switched from hydrogen to argon (Figure 3b in the maintext).

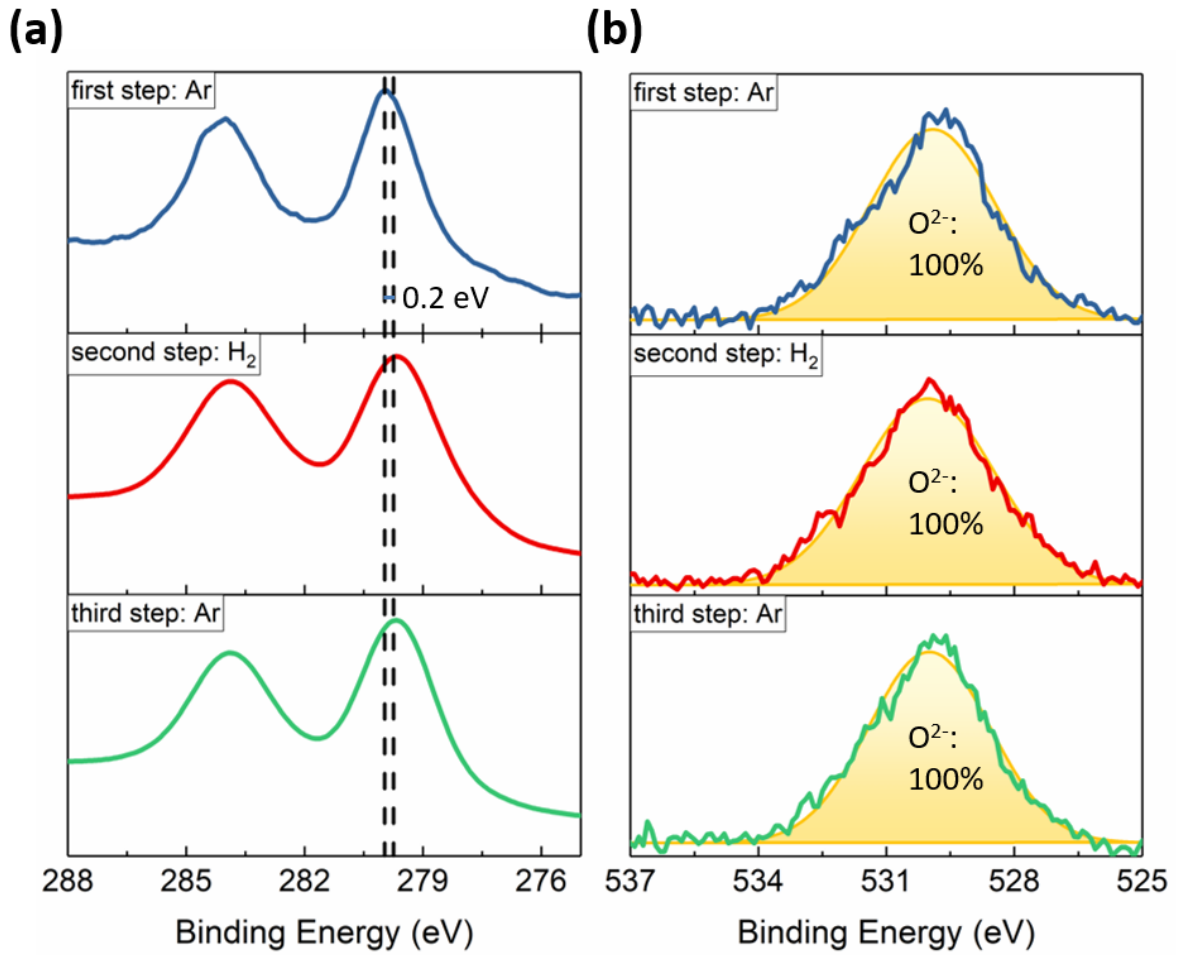

Figure S12. In-situ AP-XPS for Ru/MgO(110) under 1 mbar Ar and H_2 at 350 ^{o}C: (**a**) Ru 3d. (**b**) O1s spectra.

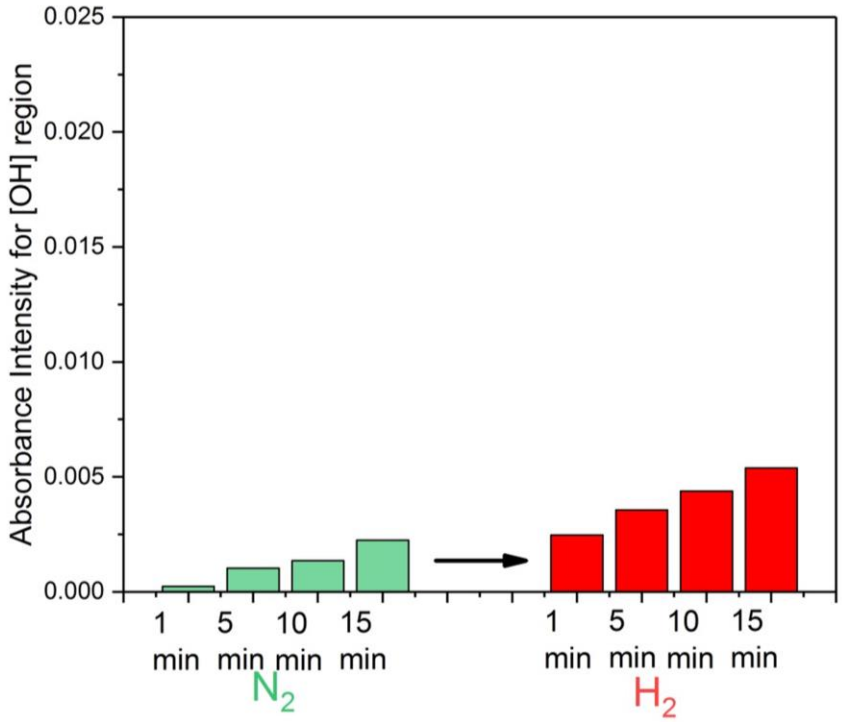

Figure S13. In-situ DRIFT for Ru/MgO(110) under 1 bar N_2 and H_2 at 200 ºC.

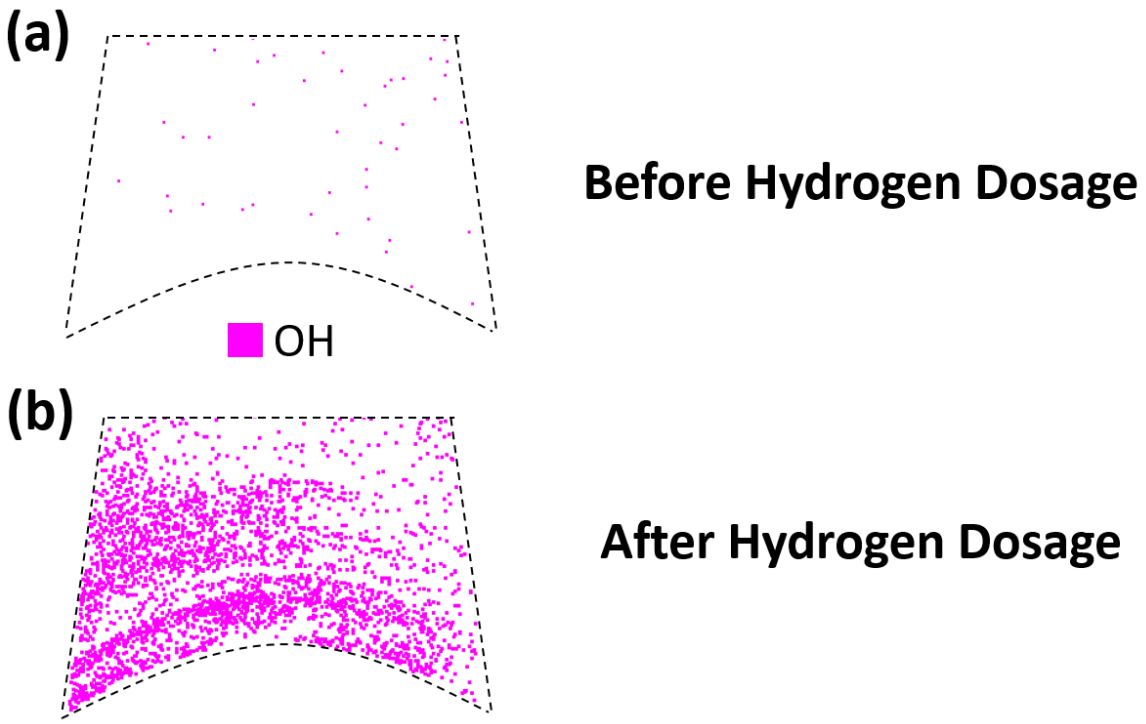

Figure S14. Atomic Probe Tomography of Ru/MgO(111) (**a**) before hydrogen dosage; (**b**) after hydrogen dosage. (Pink: OH)

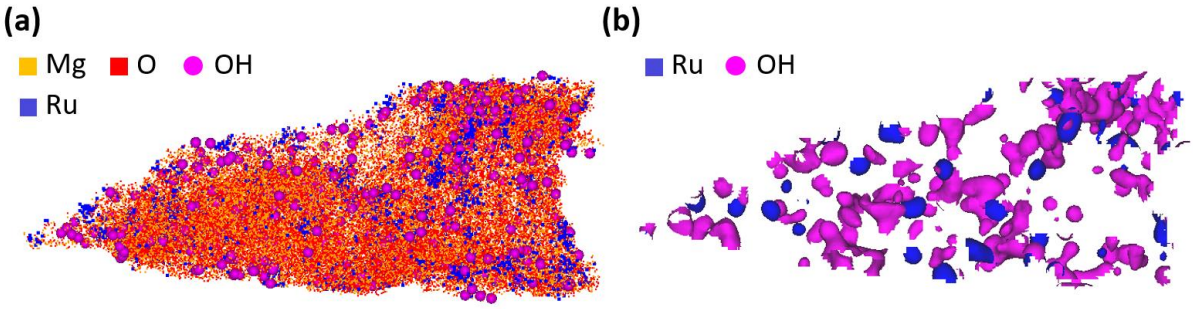

Figure S15. Atomic Probe Tomography Ru/MgO(111) (**a**) 3D atomic map of Ru, OH distribution on MgO; (**b**) Isosurface map of Ru, OH distribution (Mg: orange; O: red; Ru: blue; OH: pink)

References

(1) Verziu, M.; Cojocaru, B.; Hu, J.; Richards, R.; Ciuculescu, C.; Filip, P.; Parvulescu, V. I. Sunflower and Rapeseed Oil Transesterification to Biodiesel over Different Nanocrystalline MgO Catalysts. *Green Chem.* **2008**, *10*, 373–381.

(2) Richards, R.; Li, W.; Decker, S.; Davidson, C.; Koper, O.; Zaikovski, V.; Volodin, A.; Rieker, T.; Klabunde, K. J. Consolidation of Metal Oxide Nanocrystals. Reactive Pellets with Controllable Pore Structure That Represent a New Family of Porous, Inorganic Materials. *J. Am. Chem. Soc* **2000**, *122*, 4921–4925.

(3) Zhu, K.; Hu, J.; Kübel, C.; Richards, R. Efficient Preparation and Catalytic Activity of MgO(111) Nanosheets. *Angew. Chemie Int. Ed.* **2006**, *45*, 7277–7281.

(4) Hu, J.; Zhu, K.; Chen, L.; Kübel, C.; Richards, R. MgO(111) Nanosheets with Unusual Surface Activity. *J. Phys. Chem. C* **2007**, *111*, 12038–12044.

(5) Hu, J.; Song, Z.; Chen, L.; Yang, H.; Li, J.; Richards, R. Adsorption Properties of MgO(111) Nanoplates for the Dye Pollutants from Wastewater. *J. Chem. Eng. Data* **2010**, *55*, 3742–3748.

(6) Li, Z.; Ciobanu, C. V.; Hu, J.; Palomares-Báez, J. P.; Rodríguez-López, J. L.; Richards, R. Experimental and DFT Studies of Gold Nanoparticles Supported on MgO(111) Nano-Sheets and Their Catalytic Activity. *Phys. Chem. Chem. Phys.* **2011**, *13*, 2582–2589.

(7) Chen, J.; Tian, S.; Lu, J.; Xiong, Y. Catalytic Performance of MgO with Different Exposed Crystal Facets towards the Ozonation of 4-Chlorophenol. *Appl. Catal. A Gen.* **2015**, *506*, 118–125.

(8) Wang, F.; Ta, N.; Shen, W. MgO Nanosheets, Nanodisks, and Nanofibers for the Meerwein–Ponndorf–Verley Reaction. *Appl. Catal. A Gen.* **2014**, *475*, 76–81.

(9) Kresse, G.; Furthmüller, J. Efficient Iterative Schemes for *Ab Initio* Total-Energy Calculations Using a Plane-Wave Basis Set. *Phys. Rev. B* **1996**, *54*, 11169–11186.

(10) Kresse, G.; Furthmüller, J. Efficiency of Ab-Initio Total Energy Calculations for Metals and Semiconductors Using a Plane-Wave Basis Set. *Comput. Mater. Sci.* **1996**, *6*, 15–50.

(11) Kresse, G.; Hafner, J. *Ab Initio* Molecular Dynamics for Liquid Metals. *Phys. Rev. B* **1993**, *47*, 558–561.

(12) Perdew, J. P.; Burke, K.; Ernzerhof, M. Generalized Gradient Approximation Made Simple. *Phys. Rev. Lett.* **1996**, *77*, 3865–3868.

(13) Blöchl, P. E. Projector Augmented-Wave Method. *Phys. Rev. B* **1994**, *50*, 17953–17979.

(14) Kresse, G.; Joubert, D. From Ultrasoft Pseudopotentials to the Projector Augmented-Wave Method. *Phys. Rev. B - Condens. Matter Mater. Phys.* **1999**, *59*, 1758–1775.